



# Occlusions and their relationship with the distribution of contrasts in natural images

Rosario M. Balboa, Norberto M. Grzywacz \*

*Smith-Kettlewell Eye Research Institute, 2318 Fillmore Street, San Francisco, CA 94115-1813, USA*

Received 16 November 1999; received in revised form 11 March 2000

## Abstract

An Information-Theory-like hypothesis recently proposed for early visual processing (the Minimal Local-Asperity hypothesis) accounts for the adaptive behavior with intensity of horizontal cells. It has been shown that for this to hold, the probability that a point is traversed by an occluding border must increase supralinearly (that is, with a positive second derivative) as a function of contrast. We test this condition by analyzing the distribution of contrasts and their relationship with occluding borders in natural images. We find that the distribution of contrasts in natural images falls exponentially as a function of contrast. Moreover, the probability that a point is traversed by an occluding border in natural images always rises with contrast until reaching one. This rise tends to be supralinear and addition of noise (at low intensities) increases the supralinearity, shifting the rising portion of the curve towards higher contrasts. These findings lend support to the Minimal Local-Asperity hypothesis, which proposes that one of the main roles of early retinal processing is to extract optimally edge, contrast, and luminance attributes from the visual world based on previous knowledge about natural images. © 2000 Elsevier Science Ltd. All rights reserved.

*Keywords:* Occlusion; Distribution of contrasts; Natural images; Quantal noise; Edge localization

## 1. Introduction

The visual system extracts information from the environment. It has been argued that this information has a statistical character (Barlow, 1961a,b; Field, 1987; Barlow, 1989; Marroquin, 1995), and accordingly, several authors proposed information-optimizing theories for the goal of early visual processing (Srinivasan, Laughlin & Dubs, 1982; Atick & Redlich, 1992; Field, 1994; McCarthy & Owen, 1996; Balboa & Grzywacz, 2000a). In most of these theories, the image redundancies eliminated by the visual system are second-order statistics of the image (spatial autocorrelation or power spectrum). In another theory (Field, 1994; Balboa & Grzywacz, 2000a), the goal is to obtain a signal with the largest kurtosis possible, which would highlight the image distribution's outliers that are assumed to contain the relevant information.

We recently tested whether the above theories would explain the lateral-inhibition adaptation of horizontal cells to light intensity (Balboa & Grzywacz, 2000a). Using electrophysiological and morphological methods in two species (rabbit and goldfish) Xin and Bloomfield (1999) and Jamieson (1994) showed that the extent of lateral inhibition mediated by horizontal cells displays a bell-shape behavior as intensity increases. At low intensities, the lateral-inhibition extent was narrow and increased with intensity (Xin, Bloomfield & Persky, 1994; Xin & Bloomfield, 1999) until reaching a maximum. After this maximum, the lateral inhibition's extent narrowed down with intensity (Baldrige & Ball, 1991; Myhr, Dong & McReynolds, 1994; Lankheet, Rowe, Van Wezel & van de Grind, 1996). Analytical and computer-simulation results showed that none of the theories could explain the bell-shape behavior of horizontal cells with intensity. All these theories predicted a fall of the lateral-inhibition extent as a function of intensity (Balboa & Grzywacz, 2000a).

To explain the bell-shape behavior of the horizontal cells' lateral-inhibition extent, we recently proposed an alternate hypothesis called the Minimal Local-Asperity

\* Corresponding author. Tel.: +1-415-5611795; fax: +1-415-3458455.

*E-mail addresses:* rbalboa@ski.org (R.M. Balboa), nmg@ski.org (N.M. Grzywacz).

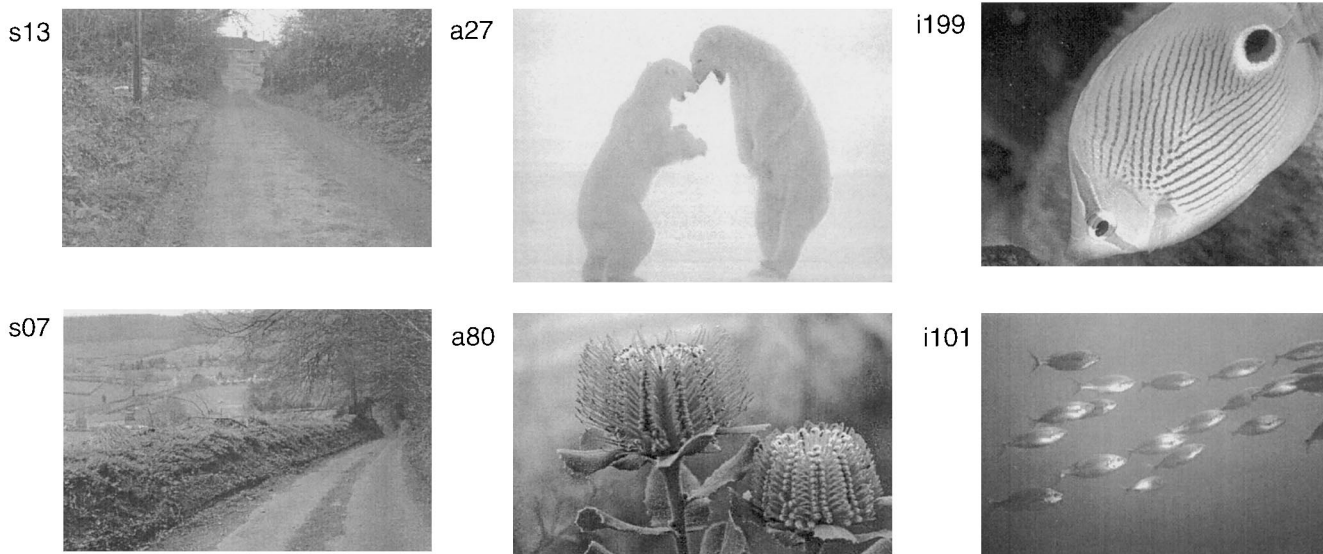


Fig. 1. Six examples of images used in this work. In this figure, while Images s13 and s07 were from the Sowerby database, the others were atmospheric and underwater images from the WWW. Source: images s13 and s07: [www.ski.org/nmgrzywaczlab/](http://www.ski.org/nmgrzywaczlab/); image a27: [www.amerisites.com/preserv2.html;filename:wld-16.jpg](http://www.amerisites.com/preserv2.html;filename:wld-16.jpg); image a80: [www.euronet.nl/users/mbleeker/fotom-e.html](http://www.euronet.nl/users/mbleeker/fotom-e.html); photo title: *Banksia coccinea*; image i199: [www.coralcay.org/cgi-bin/photos/](http://www.coralcay.org/cgi-bin/photos/); image i101: [www.repost.com/uw-photos/gallery/images/ssarpa2.jpg](http://www.repost.com/uw-photos/gallery/images/ssarpa2.jpg)

hypothesis (Balboa & Grzywacz, 2000b). With it, we obtained a bell-shape behavior qualitatively similar to the experimental results. (Elsewhere (Balboa & Grzywacz, 2000a), we stressed the differences and similarities between this hypothesis and the theories that maximize extraction of luminance information.) In the general framework of this hypothesis (Grzywacz & Balboa, 2000), the visual system would optimize the lateral inhibition's extent to minimize the error in estimating desired image attributes, based on previous knowledge about natural images and the biological processes involved. We proposed that three important attributes partially computed by the retina's outer plexiform layer (OPL) are occluding borders, their local contrasts, and the mean intensity inside visual objects. In the application of the new hypothesis to natural images, it was assumed that points with high contrast have more probability to be occluding borders than points with low contrasts. For this application, we approximated the probability of points being occluding borders as a power function of the ratio between the gradient of intensity levels and the local mean intensity (this ratio being the local contrast). In the simulations, we found that only powers larger than two could yield a bell-shape behavior for our sample of natural images. In other words, the hypothesis could only account for the biology if the probability of occluding borders as a function of contrast was supralinear, that is, had positive first and second derivatives.

In this paper, following the new hypothesis' precepts, we analyze the probability of occluding borders as a function of contrast and the distribution of contrasts in

natural images. Because of the interest in different light levels, it is also studied how these functions are affected by noise. Part of this study appeared previously in abstract form (Balboa & Grzywacz, 1998).

## 2. Methods

Twenty-nine well-calibrated images (Mackeown, 1994) were obtained from the Sowerby Research Centre (British Aerospace). These images were a subset of the Bristol Image Database, which consists of over 350 color images of a wide range of urban and rural scenes. This database was constructed with the goal to recognizing roads in a wide range of scenes. Each image contained a road; two thirds of the image were taken from an 'on-road' position and the remainder from an 'off-road' position. To determine whether calibration or human-made objects affect the results, 89 natural underwater and atmospheric images from the world wide web (WWW) were also analyzed following criteria used by other authors (Field, 1987, 1994), we selected www images without human-made objects or human-made artifacts, and with sizes greater than  $300 \times 300$  pixels. Four examples of these images and two examples of Sowerby images appear in Fig. 1.

### 2.1. Probability of occluding borders (POB) as a function of contrast

We analyzed six of the 29 calibrated images and 16 of the 89 images from the www (nine underwater and

seven atmospheric) to compare contrasts in occluding borders and outside them. (As explained below, all 118 images were used in the analysis of the distribution of contrasts.) The definition of contrast was the absolute value of the ratio between the gradient of intensity and the local intensity (see Balboa & Grzywacz, 2000b for methods and justification). To test whether high contrasts not belonging to occlusions but to camouflage markings would change the POB, we also accepted as ‘occluding’ borders the borders of a fish’s stripes for one image (i199; see Fig. 1). This latter, less strict definition of occluding border did not yield different results from the other 21 images.

The analysis of the POB in the 22 images used a psychophysical method based on a random sample of points. The computer presented the natural image with a colored dot randomly placed on it (Fig. 2). The observer (one of the authors; RMB) had to judge

whether the dot fell over an occluding border<sup>1</sup>. The computer saved the dot’s image position, local contrast, and the observer’s answer. At least 4000 dots were inspected for each image. To increase the program speed, some images were concentrically cropped, with the smallest image size used containing  $512 \times 512$  points. The data were arranged in contrast bins and the POB-contrast curves were computed as the number of occluding borders in each bin divided by the total number of points there. After this, each POB-contrast curve was smoothed with a spline.

To study the effect of noise on the POB-contrast curves, we added noise to the images as described by Balboa and Grzywacz (2000a). Using the points stored during the analysis of the images without noise, we recalculated the contrast with noise and the POB-contrast curves as above. This noise had a Poisson distribution to simulate the effects of low-light intensity (Fuortes & Yeandle, 1964; Lillywhite, 1977; Baylor, Lamb & Yau, 1979; Grzywacz, Hillman & Knight, 1988).

## 2.2. Distribution of contrasts

For each one of the 118 images, we extracted the distribution of contrast. These distributions were arranged in frequency histograms. As we will see in Section 3, these histograms almost always rose and fell with contrast at low and high contrasts respectively. The logarithm of the absolute frequency as a function of contrast was linearly fit at high contrasts. This fit was obtained for the range between the median contrast and the 99 percentile of the distribution. From the linear fits of the distributions, we extracted the slopes and correlation coefficients. Other statistics extracted from the distributions of contrast were the median contrast and the peakedness at their beginning. The peakedness was defined as the ratio between the maximal frequency and the frequency at zero contrast. Hence, the peakedness was one if there was no peak (at a contrast larger than zero) and increased monotonically with the depth of the peak. To test whether there are differences between calibrated and uncalibrated images, we statistically compared the slope, correlation coefficient, median contrast, and peakedness for the www atmospheric images against those from the Sowerby database.

## 3. Results

Fig. 3 shows the probability of occluding borders

<sup>1</sup> Occasionally, the dot fell on a position where the contrast was too low to see an occluding border, but which by contour extension probably had a real border. In those cases, the observer judged the point to be in an occluding border. If the observer was unsure whether the point was in an occluding border, then the computer selected the answer at random. Only about 10% of the points belonged to this ‘doubt’ category.

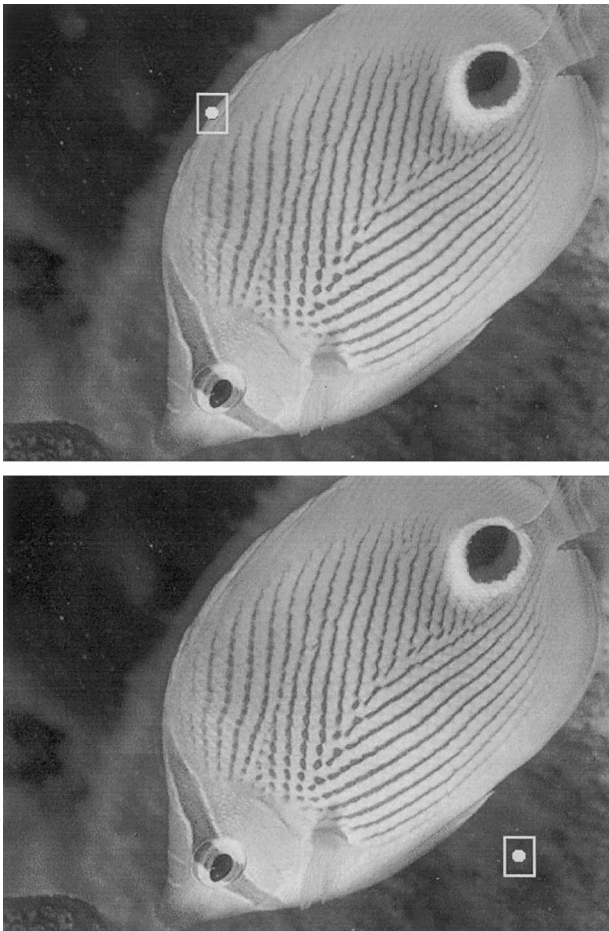


Fig. 2. The psychophysical method to obtain the POB as a function of contrast. Upper panel. The dot fell on an occluding border (in this case, where the fish occludes the background). Lower panel. The dot did not fall on an occluding border. In both panels, the dot was enlarged for clarity, but in the experiment, the dot was one pixel wide.

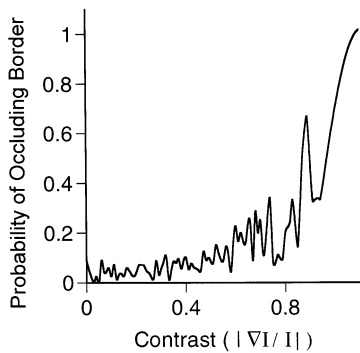


Fig. 3. Probability that an occluding border (POB) traverses a point as a function of its contrast. This probability is nearly zero for low contrasts and then tends to rise supralinearly towards one at higher contrasts.

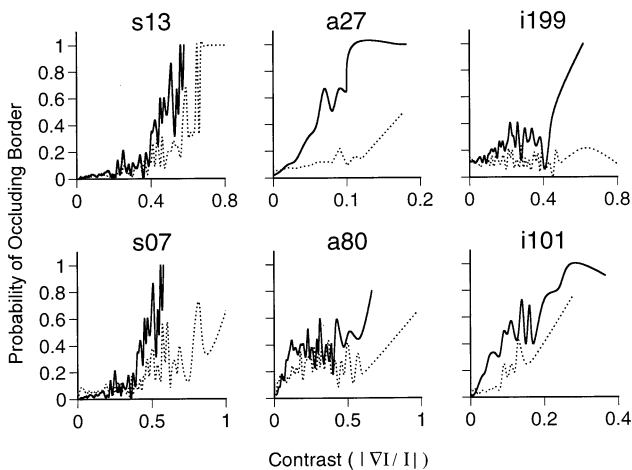


Fig. 4. POB as a function of contrast for six natural images. All curves (solid lines) presented a supralinear rise (in one or two phases) that varied from image to image. For the vast majority of the images, the curves rose all the way up to one. In the presence of noise (dotted lines), all POB-contrast curves presented a more supralinear shape (that is, with a higher threshold), which again varied from image to image. In this figure, these results were very apparent for Images s13, s07, a27, and a80. Image i101 led to a supralinear shape, which was not prominent before the addition of noise. For Image i199, the noise produced strong suppression of the POB.

(POB) as a function of contrast for one image. It is apparent that the POB rises as a function of contrast (except for relatively small fluctuations). This rise is supralinear in that it seems to have positive first and second derivatives. At low contrasts, the POB is close to zero, but it starts to increase at intermediate contrasts, often reaching one at the highest contrasts.

The supralinear trend was observed in all images, though the amount of supralinearity varied from image to image (Fig. 4). In a few cases, this supralinearity was clear and began at zero contrast (Fig. 4, Images s13, s07, and a27). In other cases, the POB-contrast curve was more similar to an oscillating (noisy) plateau at low contrasts, with a sudden rise at higher contrasts (Fig. 4, Image i199). There were also cases for which the supra-

linearity appeared in two levels (Fig. 4, Image a80). The minority of the cases displayed a more linear shape at low contrasts (Fig. 4, Image i101;<sup>2</sup>). For all images, after adding noise, the POB-contrast curve became even more supralinear and its rising portion shifted towards higher contrasts (Fig. 4, dotted lines).

That the probability that a point has an occluding border increases supralinearly with contrast does not mean that there are more occluding borders at high contrasts than at low ones. Using the same data as in Fig. 4, Fig. 5 shows that the contrary holds. This figure displays the frequency of points traversed (thick lines) and not-traversed (thin lines) by occluding borders as a function of contrast. In all images, as contrast increases, these frequencies tend to fall. In addition, the amount of non-occluding points is larger than that of the occluding borders over almost the entire range of contrasts. However, this difference tends to disappear and invert at large contrasts, explaining the rise of the POB-contrast curves. Interestingly, the shape of the distribution of contrasts at occluding borders is observed to be diverse. This distribution is almost independent of contrast in some cases (Fig. 5; Images s13, s07, and i101). However, the distribution falls sharply with contrast in others cases (Fig. 5; Images a27, a80, and i199). Finally, besides the fall with contrast at intermediate and high contrasts, there is a small but significant rise at low contrasts. We will address this rise in Section 4.

Fig. 6 displays six examples of the distribution of contrasts in our ensemble of images. Five out of these six images yielded a small peak at low contrasts. Over

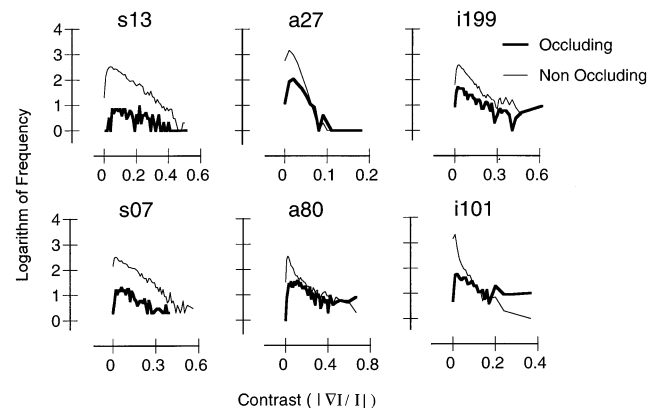


Fig. 5. Distribution of contrasts at occluding and non occluding points obtained from the same data in Fig. 4. After a fast rise at low contrasts, these distributions tend to fall with contrast. The frequency of non-occluding points dominates at low and intermediate contrasts, but the frequency of occluding points overtakes its counterpart at high contrasts.

<sup>2</sup> Nevertheless, even this image elicited a prominent supralinearity in the contrast range  $[0, 0.02]$ , which is hard to see in this figure. One cannot neglect this supralinearity, since it occurs at the contrasts of the majority of the points.

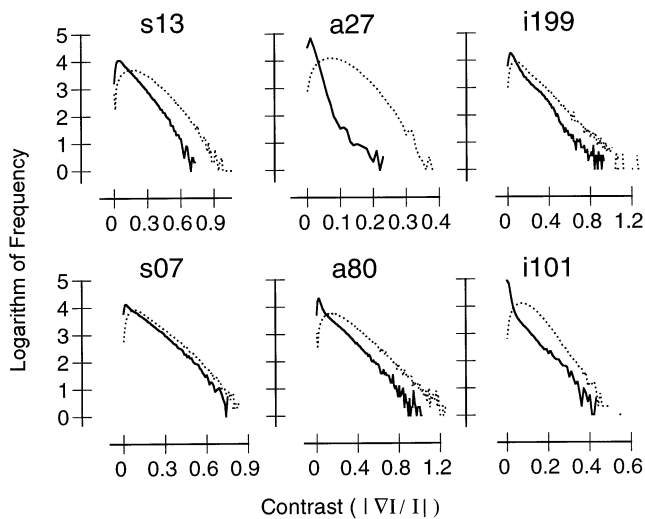


Fig. 6. Distribution of local contrasts when adding low light-level Poisson noise to the images (dotted lines) and without noise (solid lines). As in Fig. 5, after a fast rise at low contrasts, these distributions tend to fall with contrast. This fall is approximately exponential. With noise, all distributions have larger low-contrast peaks than before and the falling portion of the distributions present a shift towards higher contrasts.

all images, this peak was present in 73% of them. At contrasts higher than that of the peak, the distribution of contrasts fell linearly on a semi-log scale, which means roughly an exponential fall as a function of contrast (correlation coefficient  $-0.985 \pm 0.03$ ; mean  $\pm$  standard deviation). Adding low-light-intensity noise caused the contrast distribution to fall even more linearly on the semilog scale at high contrasts and shifted the falling portion of the curves toward higher contrasts (Fig. 6, dotted lines). With added noise, all images yielded a peak at low contrasts. The peaks for the images with noise were more pronounced than without noise. The amount of noise needed to change the shape of the distributions of local contrast was much higher than that required to change the POB-contrast curves.

There were no significant differences between the results obtained with the Sowerby image set and the www images. The similarity of the results held both for the POB-contrast curves and for the distribution of contrasts.

## 4. Discussion

### 4.1. Summary

The POB always rises with contrast (except for relatively small fluctuations) until reaching one. This rise tends to be supralinear, varying with image and noise. Addition of noise tends to increase the supralinearity and shift the rise towards higher contrasts. In relation to the distribution of contrasts, it typically has a small peak at

low contrasts. For contrasts higher than this peak, we find an approximately exponential fall as a function of contrast. Consequently, in a semilog scale, the distribution of contrasts falls linearly. We analyzed the slope of the linear fit to this fall, and the median contrast and peakedness of this distribution. Low light-level noise tended to increase the peakedness of the distribution of contrasts, make its fall more exponential, and increase its median contrast. Comparing the amount of noise needed to change the POB-contrast curve and the distribution of contrasts, we observed that the former was more affected by noise than the latter.

### 4.2. Limitations

Before interpreting our results on the POB-contrast curves and the distribution of contrasts, we wish to comment on some of the limitations to their validity. First of all, one must consider limitations imposed by the method used to deal with uncertainties on the location of occluding borders (see Footnote 1). The existence of low-contrast occluding borders are sometimes inferred by contour extension. Such an extension can cause an over-estimation of the POB at low contrasts. This is because points of low contrast that are not on occluding borders can erroneously be counted as being on occluding borders more often than points that actually are on occluding borders not be counted. There are two reasons for that: First, almost all low-contrast points are not on occluding borders (Fig. 5). Therefore, it is more likely to misclassify them than those points that are on occluding borders. Second, the human visual system's hyperacuity (Westheimer & McKee, 1977; Westheimer, 1979) ensures that the observer rarely misses a point that is truly on an occluding border. The main consequence of the over-estimation of occluding borders at low contrasts is that the measured POB-contrast curves have their low-contrast portions slightly higher than they should be.

Another limitation of our results was due to some of our images being from the www. For such images, it could be that our results on the POB-contrast curve and the distribution of contrasts were affected by uncontrolled 'imperfections' of film, camera, and JPEG image storage (for a discussion of these problems see Balboa & Grzywacz, 2000b). The three main 'imperfections' to worry about were over- and under-exposure in the photography, the film's gamma of emulsion, and the loss of high spatial frequencies. However, these imperfections did not seem to have any major effects on the results. We observed for both calibrated (Sowerby) and www images the same behavior in terms of the POB-contrast curve and distribution of contrasts. For both types of images, the POB-contrast curve had a supralinear rise as contrast increased. Moreover, noise affected the curve making it more supralinear and shifting its median towards higher contrasts. And for the distributions of contrasts, both

types of images yielded a low-contrast peak, which was enhanced by noise. At contrasts higher than this peak, the distribution of contrasts fell approximately exponentially regardless of the image's type. However, detailed inspection of the images revealed that the problems mentioned above were present. These problems caused minor differences between the www and Sowerby images. For instance, we found that the slopes of the distributions of contrast from the Sowerby images ( $-5.328 \pm 0.215$ ) were slightly steeper than those from the atmospheric WWW images ( $-4.6 \pm 0.795$ ; one-sided Mann–Whitney test,  $U = 344$ ,  $z$  corrected for ties =  $-3.701$ ,  $P < 0.001$ ).

#### 4.3. A model for the POB-contrast curve and the distribution of contrasts

We will now propose a simple one-dimensional (1D), stepwise model of the image, which accounts for the natural POB-contrast curve and the distribution of contrasts. The power of this model stems from its previous explanation of other statistical properties of natural images (Balboa & Grzywacz, 2000b; Balboa, Tyler & Grzywacz, 2000). For instance, the model accounts for why the power spectrum of natural images falls as the square of the spatial frequency (Balboa et al., 2000). In this model, there are two underlying distributions, one of the true contrasts at occluding borders and the other of noise-induced contrasts<sup>3</sup>. Because both distributions affect occluding borders, they have a wider distribution of contrasts than points outside borders. This wide distribution ensures that the POB rises to one at high contrasts. The details of the rise, such as the shape of the supralinearity, depends on the mathematical properties of the underlying distributions. These properties are addressed in the next section.

##### 4.3.1. Formulation of the model

Let a 1D image, sampled at  $N$  points, consist of  $M + 1$  regions of uniform intensity, such that the intensity profile of the  $j$ th region is

$$I_j(x) = \begin{cases} 0 & x < x_j, x > x_{j+1} \\ \hat{I}_j & x_j \leq x \leq x_{j+1} \end{cases} \quad (1)$$

where the constant  $\hat{I}_j > 0$  is  $\hat{I}_j = \bar{I} + I_j^*$ , with  $\bar{I}$  being the mean intensity across the image and  $I_j^*$  being drawn from  $P_I(I_j^*|\bar{I})$  a probability distribution with zero mean, and where  $x_j$  is obtained from some pre-specified, arbitrary distribution of sizes of regions. Therefore, the image is

<sup>3</sup> We are not taking into account contrast due to lighting (such as those from reflectances and shadows), because they are the minority in the image (Elder, Beniaminov & Pintilie, 1999).

$$I(x) = \sum_{j=1}^M I_j(x) \quad (2)$$

We now make three reasonable simplifying assumptions about the image: First,  $N \gg M$ . This inequality is reasonable, since there are many more points inside objects than at their borders. Second, if  $\beta\bar{I}$  is the standard deviation of  $P_I$ , then  $\beta\bar{I} \ll \bar{I}$ . This is equivalent to saying that the contrasts in natural images are low, for which there is much evidence (Ruderman & Bialek, 1994). Third, if  $\sigma_n$  were the standard deviation of the quantal noise in an homogeneous image of intensity  $\bar{I}$ , then  $\sigma_n \ll \bar{I}$ . Because quantal noise in images has a Poisson distribution (Fuortes & Yeandle, 1964; Lillywhite, 1977; Baylor et al., 1979; Grzywacz et al., 1988),  $\sigma_n \ll \bar{I}$ , where  $\alpha$  is a constant. Hence, the third assumption is  $\sigma_n \ll \bar{I}^{1/2}$ , that is, the intensity is sufficiently high. One consequence of this assumption is that to a good approximation the distribution of the quantal noise around the mean ( $P_Q(I|\bar{I})$ ) is Gaussian:

$$P_Q(I|\bar{I}) = \frac{1}{\sqrt{2\pi\alpha\bar{I}}} e^{-I^2/(2\alpha\bar{I})} \quad (3)$$

A consequence of the second assumption is that the noise in the different regions expressed by Eqs. (1) and (2) is similar. Therefore, we neglect the noise differences across regions and take Eq. (3) to govern the noise everywhere. In this paper, we will also model  $P_I$  as a Gaussian distribution:

$$P_I(I|\bar{I}) = \frac{1}{\sqrt{2\pi\beta\bar{I}}} e^{-I^2/(2\beta^2\bar{I})} \quad (4)$$

Some support for such a model comes from the 'occluding' lines in Fig. 5, but as we discuss below, our conclusions do not depend strongly on this choice. In Eq. (4), the variance is proportional to  $\bar{I}^2$ , since as the background intensity rises, the fluctuations from the mean increase proportionally to keep the contrasts constant. (Contrasts must remain constant, because the reflectances of objects do not vary with intensity.)

Let  $D_n(C|\bar{I})$  be the distribution of contrasts due to noise and  $D_b(C|\bar{I})$  be the distribution of contrasts due to occluding borders. The distribution of contrasts is

$$D(C|\bar{I}) = D_n(C|\bar{I}) + D_b(C|\bar{I}) \quad (5)$$

while the POB-contrast curve is

$$P_O(C|\bar{I}) = \frac{D_b(C|\bar{I})}{D_n(C|\bar{I}) + D_b(C|\bar{I})} \quad (6)$$

Consequently, the key quantities to compute from the model are  $D_n$  and  $D_b$ . Because  $N \gg M$ , points away from the border dominate  $D_n$ . Hence,  $D_n$  is just the fraction of  $N$  with contrast  $C$  due solely to noise, that is,

$$D_n(C|\bar{I}) = N \cdot P_n(C|\bar{I}) \quad (7)$$

where  $P_n(C|\bar{I})$  is the probability that in two neighbor

points, the contrast is  $C$  due to noise. In keeping with our definition of contrast in Section 2, we define the 1D contrast as  $C \approx |I_L - I_R|/I\Delta x$ , where  $I_L$  and  $I_R$  are the intensities of the left and right neighbor points respectively, and  $\Delta x$  is the distance between them. Because Eq. (3) governs the noise everywhere (see discussion after that equation), it follows that

$$P_n(C|\bar{I}) = 2\bar{I} \int_I P_Q(I|\bar{I}) P_Q(I + \bar{I}C|\bar{I}) \quad \text{if } C > 0 \quad (8)$$

and half that if  $C = 0$ , where the factor of 2 is to take into account that positive and negative instances of  $I_L - I_R$  can yield the same contrast. Substituting Eq. (3) for  $P_Q$  in Eq. (8), one gets

$$P_n(C|\bar{I}) = \sqrt{\frac{\bar{I}}{\pi\alpha}} e^{-\bar{I}C^2/4\alpha} \quad \text{if } C > 0 \quad (9)$$

and half that if  $C = 0$ .

We now calculate  $D_b(C|\bar{I})$ . As for  $D_n$ ,  $D_b$  is the fraction of the number ( $M$ ) of occluding borders with contrast  $C$ , that is,

$$D_b(C|\bar{I}) = M \cdot P_b(C|\bar{I}) \quad (10)$$

where  $P_b(C|\bar{I})$  is the probability that in two neighbor points, the contrast is  $C$  due to both an occluding border and noise. Now,  $I_L$  and  $I_R$  come from a combination of  $P_Q(I|\bar{I})$  and the distribution of image intensities,  $P_I(I|\bar{I})$ . Thus,

$$P_b(C|\bar{I}) = 2\bar{I} \int_{I_L} \int_{\varepsilon_L} \int_{I_R} P_I(I_L^T|\bar{I}) P_Q(\varepsilon_L) P_I(I_R^T|\bar{I}) \times P_Q(I_L^T + \varepsilon_L - I_R^T - C\bar{I}|\bar{I}) \quad \text{if } C > 0 \quad (11)$$

and half that if  $C = 0$ . Substituting Eqs. (3) and (4) for  $P_Q$  and  $P_I$  respectively, one obtains

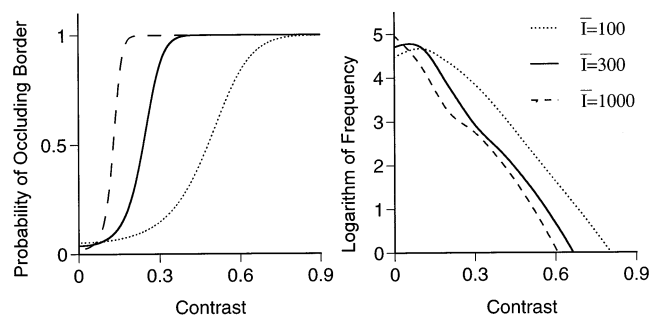


Fig. 7. Results of the model for the POB-contrast curve (Eq. (14)) and the distribution of contrasts (Eq. (13)) parametric on mean light intensity ( $\bar{I}$ ). The others parameters to obtain these curves are  $N = 10^4$ ,  $\alpha = 1$ ,  $\beta = 0.1$ , and  $f = 0.08$ . The POB-contrast curves rise supralinearly from nearly 0 to 1 and as the intensity falls, they shift toward higher contrasts. In turn, the distribution of contrasts falls approximately exponentially with contrast after a noise-induced peak or plateau at low contrasts. As in the case of the POB-contrast curve, the distribution of contrasts shifts toward higher contrast as the intensity drops.

$$P_b(C|\bar{I}) = \sqrt{\frac{\bar{I}}{\pi(\alpha + \beta^2\bar{I})}} e^{-C^2\bar{I}/4(\alpha + \beta^2\bar{I})} \quad \text{if } C > 0 \quad (12)$$

and half that if  $C = 0$ .

From Eqs. (5), (7), (9), (10) and (12), the distribution of contrasts is

$$D(C|\bar{I}) = N \sqrt{\frac{\bar{I}}{\pi}} \left[ \sqrt{\frac{1}{\alpha}} e^{-C^2\bar{I}/4\alpha} + f \sqrt{\frac{1}{\alpha + \beta^2\bar{I}}} e^{-C^2\bar{I}/4(\alpha + \beta^2\bar{I})} \right] \quad \text{if } C > 0 \quad (13)$$

and half that if  $C = 0$ , where we define  $M = f \cdot N$ , with  $f \ll 1$  associating the amount of points due to occluding borders to the total amount of points in the image.

From Eqs. (6), (7), (9), (10) and (12), the POB-contrast curve is

$$P_O(C|\bar{I}) = \frac{1}{1 + f^{-1} \sqrt{1 + \frac{\beta^2\bar{I}}{\alpha}} e^{-C^2\bar{I}\beta^2/4\alpha(\alpha + \beta^2\bar{I})}} \quad (14)$$

#### 4.3.2. Results of the model on the POB-contrast curve

Plotting Eq. (14) (left panel, Fig. 7), shows that the model can account for the main features of the POB-contrast curve obtained from natural images (Figs. 3 and 4). Fig. 7 illustrates these curves' rise from near zero to one and their supralinearity, which is enhanced by reducing  $\bar{I}$ , consistently with our results (Fig. 4). One can understand how the model achieves these results almost straight from the definition of POB-contrast curve in Eq. (6). From that definition,  $P_O = 1/(1 + D_n/D_b)$ , and thus the POB-contrast curve depends on the ratio between the distribution of contrasts due to noise ( $D_n$ ) and at occluding borders ( $D_b$ ). Because the number of points at borders is much smaller than outside them ( $N \gg M$ ),  $D_n \gg D_b$  for most contrasts, which is confirmed in Fig. 5. Therefore,  $P_O \approx 0$  for most contrasts. However, while  $D_n$  only depends on noise for its contrasts,  $D_b$  depends on both noise and actual reflectance differences in the world. Consequently,  $D_b$  has a wider distribution of contrasts than  $D_n$  (formally, while the latter's standard deviation only depends on  $\alpha$  — Eq. (9) —, the former's depends on  $\alpha$  and  $\beta$  — Eq. (12)). Hence, at large contrasts,  $D_b$  overtakes  $D_n$  (Fig. 5), making  $P_O$  rise towards 1. Because this only occurs at large contrasts,  $P_O$  is supralinear. Furthermore, as noise increases (low light levels), both  $D_b$  and  $D_n$  become wider, such that higher contrasts are required for  $D_b$  to overtake  $D_n$ . This explains the higher threshold for the POB-contrast curve to rise.

#### 4.3.3. Results of the model on the distribution of contrasts

The model can also account for the main features of the distribution of contrasts obtained from natural

images. For instance, Eq. (13) can explain the approximately exponential fall of the distribution of contrasts at intermediate and high contrasts (Fig. 6; see also Ruderman & Bialek, 1994 and Zhu & Mumford, 1997). The right panel of Fig. 7 shows rough linear falls on a semilog scale. This apparent linear fall is due to the sum of two Gaussian falls (one due to noise and one due to occluding borders plus noise) with different spreads (as explained in Section 4.3.2). Hence, different from the supralinearity of the POB-contrast curves, the apparent exponential fall of the distribution of contrasts may depend on the details of  $P_I$ . Before this fall, at low contrasts, both the data (Fig. 6) and the model (Fig. 7) can exhibit a peak. Furthermore, this peak becomes prominent with noise. From the model, we learned that the peak is due to the condition  $C = 0$  (where  $C$  is contrast) requiring perfect equality of intensities around a point in space, whereas the condition  $C > 0$  only requires that the equality is broken, which can occur in one of several directions in 2D space (see factor of half in the 1D Eqs. (8), (9), (11) and (12)). When the noise increases, perfect equality and thus  $C = 0$  becomes rarer. Another effect of noise is to shift the falling portion of the distribution of contrasts toward higher contrasts (Figs. 6 and 7). This is not surprising, since noise widens  $D_n$  and  $D_b$ , by increasing the intensity fluctuation at occluding borders and away from them.

#### 4.4. Implications for retinal biology

In recent years, several authors advanced information-optimizing theories of early visual processing based on a host of natural-image statistics, including contrast (Srinivasan et al., 1982; Atick & Redlich, 1992; Field, 1994; McCarthy & Owen, 1996; Balboa & Grzywacz, 2000a). Our results on the POB-contrast curve and the distribution of contrasts have implications for these theories and their applicability to retinal processing. For instance, some theories use the mean contrast as a parameter (Srinivasan et al., 1982; Atick & Redlich, 1992). Although analysis of these theories (Balboa & Grzywacz, 2000a) show that they cannot account for the adaptive behavior of retinal horizontal cells (Xin & Bloomfield, 1999), the possibility remains that these theories could be successfully modified.

The results on the POB-contrast curve in this paper have particular relevance for another information-optimizing hypothesis, the Minimal Local-Asperity hypothesis (Balboa & Grzywacz, 2000b; Grzywacz & Balboa, 2000). This hypothesis accounts successfully for the adaptation behavior of the lateral inhibition mediated by horizontal cells (Xin & Bloomfield, 1999). To do so, the hypothesis requires natural images to yield supralinear POB-contrast curves (Balboa & Grzywacz, 2000b). Because this is exactly what one finds (Figs. 3 and 4), this paper lends support to the Minimal Local-Asperity hypothesis. Hence, we would like to conclude by propos-

ing a goal for early retinal lateral inhibition based on the POB's findings described here and the Minimal Local-Asperity hypothesis (see Balboa & Grzywacz, 2000a for a comparison between the Minimal Local Asperity Hypothesis and other theories that try to maximize extraction of luminance information). Deciding whether a point lies on an occluding border by visual means can be a difficult task. It may involve learning early in development and almost certainly, has applied significant evolutionary pressure on the visual system. The right decision varies at each instant with the statistics of the varying visual habitat, including illumination level, contrast, and sizes of objects. Therefore, adaptive mechanisms are necessary to adjust the animal's early visual system to its environment. We propose based on our hypothesis that such adaptation modifies horizontal cells' receptive fields to deal optimally with different intensities and habitats. To achieve such an optimality, that is, to minimize the number of errors in performing the desired tasks (for instance, edge extraction, and contrast and intensity measurements), the visual system must use relevant statistical knowledge about natural images. In the case of the Minimal Local-Asperity hypothesis, the required knowledge is the POB-contrast curve. Therefore, we propose that armed with this knowledge, the early retinal lateral-inhibition process contributes to edge and contrast extraction with minimal noise and avoiding as much as possible the straddling of occluding borders.

#### Acknowledgements

We thank Dr Andrew Wright for allowing us to use the Sowerby Image Database (British Aerospace), and Drs Alan Yuille and Scott Konishi for sharing with us their TIFF version of the images from this database. We also thank Dr Joaquín De Juan and Dr Russell Hamer for critical comments, and Dr José Oncina for support during RMBs Ph.D. work at the University of Alicante, Alicante, Spain. This work was supported by National Eye Institute Grants EY08921 and EY11170, and the William A. Kettlewell Chair to NMG, by Grant TIC97-0941 to Dr José Oncina, and by the National Eye Institute Core Grant EY06883 to Smith-Kettlewell.

#### References

- Atick, J. J., & Redlich, A. N. (1992). What does the retina know about natural scenes? *Neural Computation*, 4, 196–210.
- Balboa, R. M., & Grzywacz, N. M. (1998). The minimal-local asperity theory of retinal lateral inhibition. *Investigative Ophthalmology and Visual Science (Supplement)*, 39, 562.
- Balboa, R. M., & Grzywacz, N. M. (2000a). The role of early retinal lateral inhibition: more than maximizing luminance information. *Visual Neuroscience*, 17, 77–90.

- Balboa, R.M., Grzywacz, N.M. (2000b). The minimal-local asperity hypothesis of early retinal lateral inhibition. *Neural Computation*, 12.
- Balboa, R.M., Tyler, C.W., & Grzywacz, N.M. (2000). Occlusions contribute to scaling in natural images. (Submitted for publication).
- Baldrige, W. H., & Ball, A. K. (1991). Background illumination reduces horizontal cell receptive field size in both normal and 6-hydroxydopamine-lesioned goldfish retinas. *Visual Neuroscience*, 7, 441–450.
- Barlow, H. B. (1961a). Possible principles underlying the transformation of sensory messages. In W. A. Rosenblith, *Sensory communication*. Cambridge: MIT Press.
- Barlow, H. B. (1961b). The coding of sensory messages. In W. H. Thorpe, & O. L. Zangwill, *Current problems in animal behavior*. Cambridge: University Press.
- Barlow, H. B. (1989). Unsupervised learning. *Neural Computation*, 1, 295–311.
- Baylor, D. A., Lamb, T. D., & Yau, K.-W. (1979). Responses of retinal rods to single photons. *Journal of Physiology*, 288, 613–634.
- Elder, J. H., Beniaminov, D., & Pinteric, G. (1999). Edge classification in natural images. *Investigative Ophthalmology and Visual Science (Supplement)*, 40, 357.
- Field, D. J. (1987). Relations between the statistics of natural images and the response properties of cortical cells. *Journal of the Optical Society of America*, 4, 2379–2394.
- Field, D. J. (1994). What is the goal of sensory coding? *Neural Computation*, 6, 559–601.
- Fuortes, M. G. F., & Yeadle, S. (1964). Probability of occurrence of discrete potentials waves in the eye of the *Limulus*. *Journal of Physiology*, 47, 443–463.
- Grzywacz, N.M., Balboa, R.M. (2000). A Bayesian theory of adaptation and its application to the retina. (Submitted for publication).
- Grzywacz, N. M., Hillman, P., & Knight, B. W. (1988). The quantal source of area supralinearity of flash responses in *Limulus* photoreceptors. *Journal of General Physiology*, 91, 659–684.
- Jamieson, M.S. (1994). *Mechanisms regulating horizontal cell receptive field size in goldfish retina*. Doctoral Dissertation. McMaster University, Hamilton, Ontario, Canada.
- Lankheet, M. J., Rowe, M. H., Van Wezel, R. J., & van de Grind, W. A. (1996). Spatial and temporal properties of cat horizontal cells after prolonged dark adaptation. *Vision Research*, 36, 3955–3967.
- Lillywhite, P. G. (1977). Single photon signals and transduction in an insect eye. *Journal of Comparative Physiology*, 122, 189–200.
- Mackeown, W.P.J. (1994). *Labelling image database and its application to outdoor scene analysis*. Doctoral Dissertation, University of Bristol.
- Marroquin, J. L. (1995). Regularization theory and low-level vision. In M. A. Arbib, *The handbook of brain theory and neural networks* (pp. 800–804). Cambridge: MIT Press.
- McCarthy, S. T., & Owen, W. G. (1996). Preferential representation of natural scenes in the salamander retina. *Investigative Ophthalmology and Visual Science (Supplement)*, 37, S674.
- Myhr, K. L., Dong, C. J., & McReynolds, J. S. (1994). Cones contribute to light-evoked, dopamine-mediated uncoupling of horizontal cells in the mudpuppy retina. *Journal of Neurophysiology*, 72, 56–62.
- Ruderman, D. L., & Bialek, W. (1994). Statistics of natural images: scaling in the woods. *Physics Review and Letters*, 73, 814–817.
- Srinivasan, M. V., Laughlin, S. B., & Dubs, A. (1982). Predictive coding: a fresh view of inhibition in the retina. *Proceedings of the Royal Society of London B*, 216, 427–459.
- Westheimer, G., & McKee, J. (1977). Spatial configurations for visual hyperacuity. *Vision Research*, 17, 941–947.
- Westheimer, G. (1979). The spatial sense of the eye. *Investigative Ophthalmology and Visual Science*, 18, 893–912.
- Xin, D., & Bloomfield, S. A. (1999). Dark- and light-induced changes in coupling between horizontal cells in mammalian retina. *Journal of Comparative Neurology*, 405, 75–87.
- Xin, D., Bloomfield, S. A., & Persky, S. E. (1994). Effect of background illumination on receptive field and tracer-coupling size of horizontal cells and AII amacrine cells in the rabbit retina. *Investigative Ophthalmology and Visual Science (Supplement)*, 35, 1363.
- Zhu, S. C., & Mumford, D. (1997). Prior learning and Gibbs reaction-diffusion. *IEEE Transactions on Pattern Analysis and Machine Intelligence*, 19, 1236–1250.